Editors' Suggestion | Featured in Physics

Observations and properties of the first laboratory fusion experiment to exceed a target gain of unity

A. Pak,[1,*] A. B. Zylstra,[1,*,†] K. L. Baker,[1] D. T. Casey,[1] E. Dewald,[1] L. Divol,[1] M. Hohenberger,[1] A. S. Moore,[1] J. E. Ralph,[1] D. J. Schlossberg,[1] R. Tommasini,[1] N. Aybar,[1] B. Bachmann,[1] R. M. Bionta,[1] D. Fittinghoff,[1] M. Gatu Johnson,[2] H. Geppert Kleinrath,[3] V. Geppert Kleinrath,[3] K. D. Hahn,[1] M. S. Rubery,[1] O. L. Landen,[1] J. D. Moody,[1] L. Aghaian,[4] A. Allen,[4] S. H. Baxamusa,[1] S. D. Bhandarkar,[1] J. Biener,[1] N. W. Birge,[3] T. Braun,[1] T. M. Briggs,[1] C. Choate,[1] D. S. Clark,[1] J. W. Crippen,[4] C. Danly,[3] T. Döppner,[1] M. Durocher,[3] M. Erickson,[1] T. Fehrenbach,[5] M. Freeman,[3] M. Havre,[4] S. Hayes,[4] T. Hilsabeck,[1] J. P. Holder,[1] K. D. Humbird,[1] O. A. Hurricane,[1] N. Izumi,[1] S. M. Kerr,[1] S. F. Khan,[1] Y. H. Kim,[3] C. Kong,[4] J. Jeet,[1] B. Kozioziemski,[1] A. L. Kritcher,[1] K. M. Lamb,[3] N. C. Lemos,[1] B. J. MacGowan,[1] A. J. Mackinnon,[1] A. G. MacPhee,[1] E. V. Marley,[1] K. Meaney,[3] M. Millot,[1] J.-M. G. Di Nicola,[1] A. Nikroo,[1] R. Nora,[1] M. Ratledge,[4] J. S. Ross,[1] S. J. Shin,[1] V. A. Smalyuk,[1] M. Stadermann,[1] S. Stoupin,[1] T. Suratwala,[1] C. Trosseille,[1] B. Van Wonterghem,[1] C. R. Weber,[1] C. Wild,[5] C. Wilde,[3] P. T. Wooddy,[1] B. N. Woodworth,[1] and C. V. Young[1]

[1]*Lawrence Livermore National Laboratory, P.O. Box 808, Livermore, California 94551-0808, USA*

[2]*Massachusetts Institute of Technology, Cambridge, Massachusetts 02139, USA*

[3]*Los Alamos National Laboratory, Mail Stop F663, Los Alamos, New Mexico 87545, USA*

[4]*General Atomics, San Diego, California 92186, USA*

[5]*Diamond Materials GmbH, 79108 Freiburg, Germany*

(Received 27 October 2023; accepted 18 January 2024; published 5 February 2024)

An indirect-drive inertial fusion experiment on the National Ignition Facility was driven using 2.05 MJ of laser light at a wavelength of 351 nm and produced 3.1 ± 0.16 MJ of total fusion yield, producing a target gain $G = 1.5 \pm 0.1$ exceeding unity for the first time in a laboratory experiment [Phys. Rev. E **109**, 025204 (2024)]. Herein we describe the experimental evidence for the increased drive on the capsule using additional laser energy and control over known degradation mechanisms, which are critical to achieving high performance. Improved fuel compression relative to previous megajoule-yield experiments is observed. Novel signatures of the ignition and burn propagation to high yield can now be studied in the laboratory for the first time.

DOI: 10.1103/PhysRevE.109.025203

I. INTRODUCTION

A laboratory fusion experiment recently produced more energy from nuclear fusion reactions than the laser energy required to drive the target giving a target gain G of 1.5 [1]. The experiment was done at the National Ignition Facility (NIF) [2] using the inertial confinement fusion approach [3] designated laser indirect drive [4]. The NIF comprises 192 individual Nd glass laser beams that provide frequency-tripled (3ω or 351 nm) light in a specified pulse shape to the target. The target consists of a cylindrical high-Z hohlraum in which the laser energy is converted to a thermal x-ray drive with a peak radiation temperature reaching approximately 300 eV. These x rays ablate the surface of a spherical capsule positioned at the center of the hohlraum. The capsule target is comprised of an outer shell of high-density carbon (HDC) ablator material which encompasses an inner shell of deuterium-tritium (DT) fusion fuel. The ablation of the outer HDC shell triggers an inward compression that at minimum volume, or stagnation, creates a high-density shell of DT fuel that surrounds a lower-density but higher-temperature central hot spot of DT plasma where fusion reactions begin to occur. Only approximately 1% of the initial laser energy is converted into the kinetic energy of the implosion that does mechanical work on the DT plasma. Each fusion reaction produces a 3.5-MeV helium ion, or an α particle and a 14.1-MeV neutron. The energy of the α particles is transferred via collisions to the DT plasma. When the rate of self-heating from the DT fusion reaction's α products exceeds the power losses of the plasma, the Lawson criterion is satisfied [5] and the plasma temperature can continue to increase. The increase in temperature further increases the rate of fusion, leading to a cascade of reactions that can produce more fusion energy than the laser energy used to initiate the process. Ultimately, the high central pressure of the reacting plasma expands outward, reducing the temperature and quenching the fusion burn.

An overview of results from this experiment is described in Ref. [1], while Ref. [6] offers details on the computational design and post-shot modeling and Ref. [7] gives additional physical theory underpinning ICF. Here we present additional data and interpretations and describe the unique features of this experiment relative to previous ones [8]. Key to achieving these results was utilizing additional laser energy, at fixed power, evidenced below in data of additional radiation drive experienced by the capsule. The additional drive allows for the use of capsule targets with thicker and more

[*]These authors contributed equally to this work.

[†]Present address: Pacific Fusion, Fremont, California 94538, USA.

massive HDC ablator layers. As will be discussed, this enables implosions to achieve higher areal densities and higher fusion yields. To realize these higher fusion yields, well-known sources of degradation must also be simultaneously controlled. Herein we describe how the low-mode asymmetry, especially modes 1 and 2, adequate for gain exceeding unity, was reached and discuss the target quality relative to previous experiments. Evidence for increased compression of the fuel, consistent with higher areal densities and fusion yields, is also discussed. Finally, at high fusion yield these experiments enter a novel physical regime that is observable for the first time in laboratory experiments with key data shown; for example, there is evidence of increasing ion temperature and decreasing burn duration, increased energy and pressure in the igniting fuel, and novel signatures in x-ray emission.

The paper is organized as follows. Section II provides details of the experimental changes made from the previous high-performing NIF experiment. Section III describes key ignition metrics important in guiding these changes and interpreting the data. Section IV presents the most important observations related to the achievement of high performance. Section V details data-driven inferences of conditions reached in the ignited hot spot. Section VI summarizes the results.

II. EXPERIMENTAL DETAILS

An implosion design called Hybrid E (HyE) [9,10] was developed over the past several years based on a strategy for achieving higher-performance implosions given in Refs. [11,12]. The physics goal of this strategy was to increase the energy coupled to the DT hot spot while maintaining energy density, which was expected to favorably improve the hot spot energy balance in the burning plasma regime. This was done by increasing the radiation drive through increasing the laser energy by 1.3–1.9× while simultaneously increasing the capsule inner radius to 1050–1100 μm from 844–910 μm used in previous high-performing three-shock implosions with HDC ablators [13]. To maintain implosion symmetry, increased levels of cross-beam energy transfer were used in conjunction with increases to the hohlraum diameter from 5.75–6.2 mm to a diameter of 6.4 mm [14–16]. These changes enhanced the amount of inner laser cone energy transmitted to the waist of the hohlraum allowing for symmetry control. Additionally, the hohlraum length was also increased from 10 to 11.2 mm. In late 2020 through early 2021, Hybrid E and I-Raum implosions produced yields in the range of approximately 100–170 kJ and reached the burning plasma regime [17,18] defined as when the heating from DT fusion produced α particles exceeds the initial PdV work done on the hot spot. This marked a significant milestone in which the self-heating begins to dominate energetically. A parallel series of NIF experiments, using a HyE 1100-μm-inner-radius capsule design, showed that reducing the size of the laser entrance hole on the hohlraum increased the radiation drive on the capsule by 7%. This enhancement was used to reduce peak power, extend the drive, and together with significant improvements in the capsule quality led to an increase in performance for a 1050-μm capsule design based on the burning plasma results, in an August 2021 NIF shot N210808 (NIF shot notation being NYYMMDD, where N = NIF, YY = year, MM = month, and DD = day when the shot countdown began) in which the hot spot exceeded Lawson's criterion for ignition [8,19,20]. The N210808 experiment produced a fusion yield of 1.3 ± 0.07 MJ with 1.89 MJ of 3ω laser light ($G \sim 0.7$).

Recent upgrades to NIF's laser capability enabled delivering an additional 8% of 3ω laser energy [21,22], which we use here to increase the hohlraum drive and implode a 7% thicker capsule. Specifically, the total energy delivered to the target increased from 1.89 MJ, as on N210808, to 2.05 MJ, as on N221204. On N221204 this increase in energy allowed for the extension of the peak laser power by 200 ps with an average peak power of 440 TW as compared to the peak power of 427 TW on N210808. Additionally, to maintain shock timing, the first shock, or foot of the laser pulse, was extended by 150 ps on N221204 versus N210808.

The key design changes implemented, as discussed in Ref. [6], were to use this higher laser energy to increase the peak radiation temperature and drive a thicker (higher ablator mass) capsule. Relative to N210808, the total thickness of the HDC ablator was increased by 6 μm (additional details on target quality are given in the Appendix). The shape of the laser pulse was also adjusted, since the thicker capsule requires a longer foot (low-amplitude portion of the laser pulse) to maintain equivalent shock timing, as the shock transit time increases through a thicker ablator. For additional details of the physics design see Ref. [6].

The measured total laser power versus time is shown in Fig. 1 for N210808 compared to N220919 and N221204. Experiment N220919 is included because it is identical to N221204 except that it had 0.25 Å less wavelength separation between the inner and outer laser cones. As will be discussed in more detail, this resulted in a more asymmetric radiation drive and a hot spot with a significant shape asymmetry and performance degradation. Both the longer foot and longer time at peak power are apparent. The time-dependent radiation drive is shown in Fig. 1(b), quantified as an equivalent blackbody radiation temperature T_{rad} measured through a laser entrance hole using the Dante 1 instrument [23–25], a multichannel soft-x-ray spectrometer. During the foot at low T_{rad} the data have a large uncertainty with this configuration, but the characteristics through the peak of the drive are clearly shown. Dante 1 did not produce data for N210808 due to a hardware problem encountered during the experiment. Instead, the blue line shows equivalent data for several subsequent shots that utilized the same laser pulse and hohlraum conditions as N210808. These results can be directly compared to the data for N220919 (orange) and N221204 (green). The additional drive at the end of the pulse is clearly manifested by a slightly higher peak T_{rad}. This demonstrates that the drive increase when using the additional laser energy. Additional analysis of the hohlraum conditions and radiation temperature are given in Ref. [26].

III. IGNITION THRESHOLD

As discussed in the companion paper [6], radiation hydrodynamic simulations indicated that to achieve higher fusion yields from the increase in laser energy at a fixed peak laser

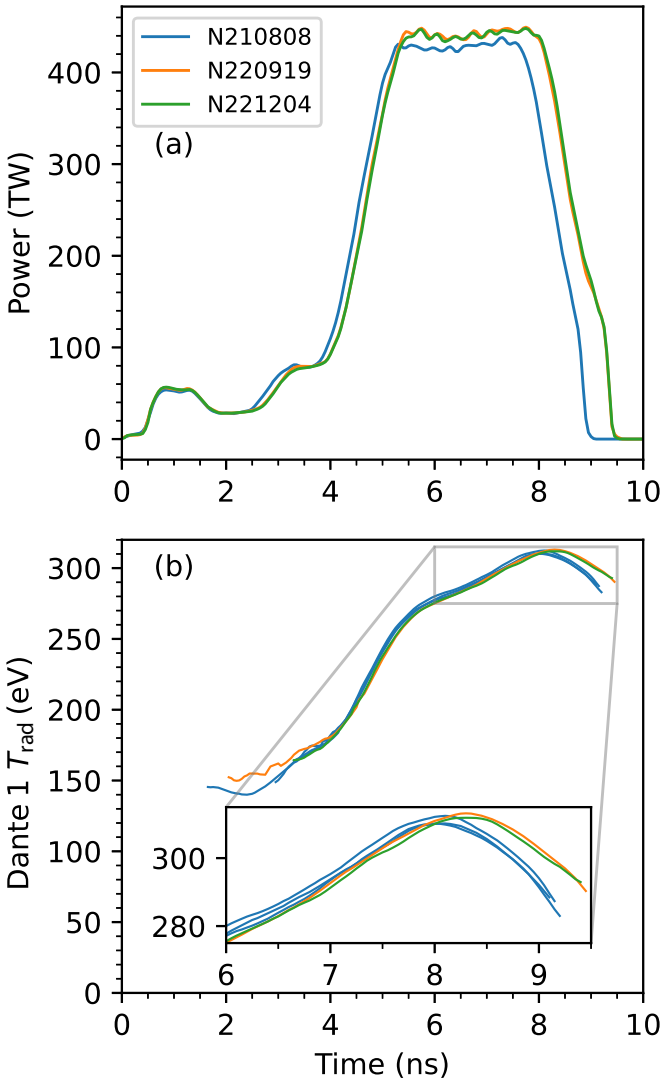

FIG. 1. (a) Laser pulses as delivered for N220919 and N221204 versus N210808. (b) Measured radiation temperature T_{rad} from Dante 1 versus time. Since the Dante 1 data are not available for N210808, data from several shots that repeated the same laser pulse are shown in blue. Dante data are shown until 100 ps before peak nuclear production.

power, an increase in the ablator thickness and therefore mass was desirable. Simulations suggested that despite the decrease in implosion velocity due to the larger implosion mass, the yield amplification Y_{amp} $(=Y/Y_{no\,\alpha})$ could be improved by increasing the areal density $\rho R = \int dr \rho(r)$ while approximately maintaining the energy coupled to the hot spot. Here $Y_{no\,\alpha}$ refers to the DT fusion yield without the presence of α-particle self-heating. This increase in fusion yield with increasing areal density is consistent with theory, for example, in Refs. [27,28], where the yield and Lawson parameter is proportional to the product of areal density, velocity, and an asymmetry degradation factor. While radiation hydrodynamic simulations include the myriad of physical processes that impact the fusion yield, it can also be instructive to parametrize the yield amplification into a few principal variables and associated observables to gain insight into the scaling of the yield.

Previous analysis describes how the yield amplification in simulations increases rapidly at the onset of ignition (e.g., Ref. [29]); this is sometimes described as the ignition cliff. One particular analysis parametrizes the yield amplification as a function of a so-called generalized ignition threshold factor (ITFX). The term $\mathrm{ITFX}_{no\,\alpha}$ is used to describe the incident conditions of the plasma and confining fuel shell that occur at minimum volume, or stagnation for an implosion in the absence of α-particle self-heating. In this model, ITFX is given by

$$\mathrm{ITFX}_{no\,\alpha} \propto \frac{Y_{no\,\alpha}}{M_{DT}} (\mathrm{DSR}_{no\,\alpha})^{2.1}. \quad (1)$$

Here M_{DT} is the DT fuel mass and Y is the yield of unscattered DT fusion neutrons. The downscattered ratio (DSR) is the ratio of neutrons downscattered by the areal density of the DT hot spot and surrounding fuel shell to energies of 10–12 MeV to the number of neutrons in the 13–15 MeV energy range. The DSR can be related to the total areal density of the DT hot spot and fuel shell $\rho R_{DT} = C \times \mathrm{DSR}$, with C a coefficient between 18 and 19 derived from static MCNP calculations and dynamic radiation hydrodynamic calculations [30]. The no α subscript indicates the value of the parameter is to be evaluated in the absence of α-particle self-heating. In this framework, ignition is defined when $\mathrm{ITFX}_{no\,\alpha} = 1$, where the hot spot conditions are sufficient to trigger a level of α-particle self-heating that can initially overcome all of the power losses from the plasma, leading to a rapid increase in the yield amplification Y_{amp}. On the ignition cliff at the current areal density, $Y_{amp} \propto \mathrm{ITFX}^5_{no\,\alpha}$ [29]. For a fixed amount of DT fuel, this indicates that relatively small changes in $Y_{no\,\alpha}$ or $\rho R_{no\,\alpha}$ can lead to large changes in the fusion performance. For example, on the ignition cliff, a 10% increase in $Y_{no\,\alpha}$ or $\rho R_{no\,\alpha}$ can lead to about a factor of 2 increase in fusion yield.

The $Y_{no\,\alpha}$ of the system can be rewritten as $Y_{no\,\alpha} \propto n^2_{DT} \langle \sigma v \rangle V \tau \propto E_{hs} T_i^{1.5} P \tau$ given that the expected temperature in the absence of α heating on the cusp of ignition is of 4.3 keV where the DT reactivity $\langle \sigma v \rangle \propto T_i^{3.5}$. Here E_{hs} is the energy coupled to the hot spot, T_i is the plasma ion temperature, P is the plasma pressure, and τ is the duration over which the burn rate can be sustained. Asymmetries in compression or increased radiative loss from a higher-atomic-number mix can reduce the energy coupled to the hot spot E_{hs} and reduce the temperature and pressure [31], lowering the $Y_{no\,\alpha}$, the $\mathrm{ITFX}_{no\,\alpha}$, and the Y_{amp}.

Within this framework, experimental observables associated with an increased $\mathrm{ITFX}_{no\,\alpha}$ and higher-yield amplifications include an increase in the areal density and the ability to achieve higher-yield amplifications than prior work despite having higher levels of observed degradations (defined below) that reduce the energy coupled to the reacting plasma.

IV. KEY DATA AND RESULTS

A. Mode 1 symmetry

A major source of performance degradation arises from implosion asymmetries having low-spatial-mode number. Here mode number refers to a spatial decomposition of hot spot shape into Legendre polynomials [32], where mode 1 and mode 2 correspond to a simple linear translation and an oblate

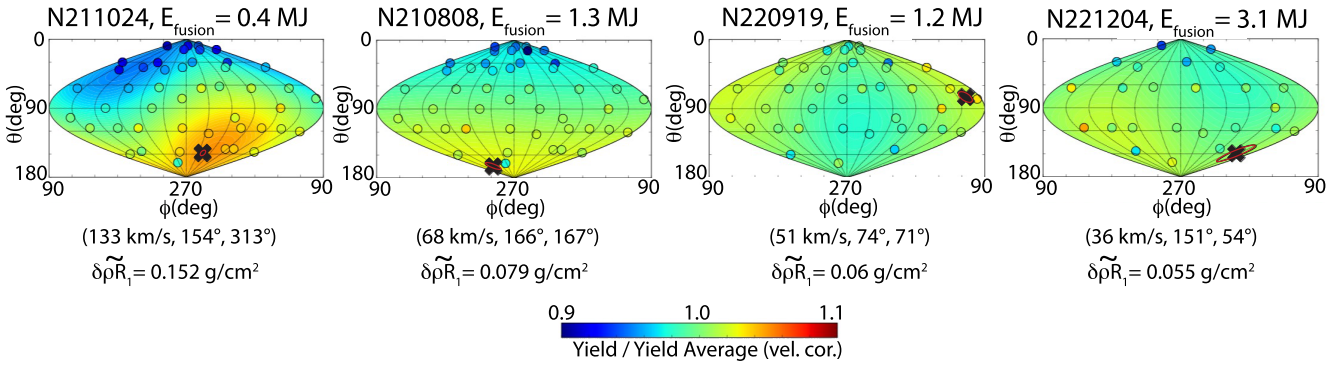

FIG. 2. Angularly resolved nuclear activation maps from a series of experiments showing a progression of reduced mode 1 symmetry impact. Shown below each plot are the hot spot velocity and inferred mode-1 ρR perturbation (modes > 1 are suppressed by RTNAD sampling effects [39]). In each panel × marks the direction of the hot spot velocity, with the red ellipse denoting the uncertainty and the circles the real-time nuclear activation diagnostic locations.

and a prolate distortion from spherical, respectively. Typical seeds for the mode 1 asymmetries include small asymmetries in the multibeam laser drive [33], capsule thickness variations [34], asymmetric hohlraum features (e.g., diagnostic windows [35,36]), and thickness variations in the cryogenic DT ice layer. Mitigating these seeds was a necessary step to reach ignition.

Figure 2 shows neutron activation data used to assess mode 1 amplitude and infer its impact on implosion performance. Figures 2(a) and 2(b) used a 1.90-MJ laser drive while Figs. 2(c) and 2(d) used 2.05 MJ; N221204 is the gain $G > 1$ implosion. The colormap shows the angular asymmetry in the 13–15-MeV neutron emission, while the overall shape represents a "sky map" of the target chamber. Each small circle shown is a measurement location of the 13–15-MeV yield using activation [37,38]. The colormap represents the spherical harmonic fit to the yield data from up to 48 locations. Here the data have been fit using up to the second mode of the spherical harmonic. The variation in the 13–15-MeV yield corresponds to asymmetries in areal density ρR around the fusing plasma. An approximation for how yield variation maps to areal density is given by $\frac{\delta Y}{Y} = -0.21\delta\rho R$, where the fractional difference in yield is proportional to the variation in ρR [39]. This estimate for the four implosions is given below each image.

Another measure of mode 1 asymmetry is the observed shifts in mean kinetic energy of the emitted neutrons. A mode 1 asymmetry gives rise to bulk motion of the hot spot leading to a translation in space; this corresponds to a Doppler shift in emitted neutron energy. By using multiple lines of sight to measure the spectrum, it is possible to resolve the bulk motion into a velocity vector [40,41]. The hot spot velocity vector (magnitude and direction) are shown below each implosion and denoted on the sky map by black crosses. This motion exemplifies residual kinetic energy that is not converted to compression and heating of the hot spot and indicates a reduction from ideal performance [27]. Recent work has found that the rapid pressure increase resulting from significant α-particle heating can amplify the observed hot spot velocities [42]. It is found that the degradation factor to the fusion yield is quadratic with observed hot spot velocity, with the fusion yield being decremented with increasing asymmetry and observed velocities. Using this relationship, it is estimated that due to the asymmetry in compression from a mode 1 source, the fusion yield for N211024 is reduced by approximately 70% while for N221204 the fusion yield is reduced by only approximately 5%.

The implosions shown in Fig. 2, moving from left to right, exhibit decreasing mode 1 asymmetries and corresponding degradation levels. As mentioned above, mitigating low-mode asymmetries was important for achieving $G > 1$. Here we have quantified the impact of mode 1 and the next section will examine the impact of mode 2 asymmetries.

B. Mode 2 symmetry

Mode 2 asymmetries can arise from an imbalance in the radiation drive between the poles and equator of the capsule. This distorts the desired spherical implosion symmetry and reduces the rate of PdV/dt work and energy coupled to the reacting plasma, reducing ITFX and the fusion yield [43,44].

As discussed, the increase in the available laser energy from 1.9 to 2.05 MJ was used to implode a capsule with an approximately 7% thicker HDC ablator layer. This was expected to achieve higher-yield amplifications by further increasing the areal density and hot spot pressure while maintaining the amount of energy coupled to the hot spot. This design change was expected to result in implosions that can reach higher fusion yields for similar or higher levels of low-mode asymmetries and mix degradations [45] as compared to the 1.9-MJ design.

By examining the observed mode 1 and mode 2 asymmetries, it becomes clear that the 2.05-MJ design can indeed achieve higher levels of fusion yield for higher levels of asymmetry than the 1.9-MJ design. Figure 3 shows neutron-emission-weighted images and how the mode 2 symmetry and fusion yield vary for pairs of experiments N211024 and N210808 and experiments N220919 and N221204, conducted with 1.9 and 2.05 MJ, respectively. The hot spot symmetry is evaluated by fitting the 17% contour of peak emission with a Legendre polynomial. The mode 2 asymmetry is quantified by taking the amplitude of the P_2 coefficient and is a measure of the ellipticity of the hot spot. The total low-mode symmetry degradation is a combination of both the mode 1, shown in

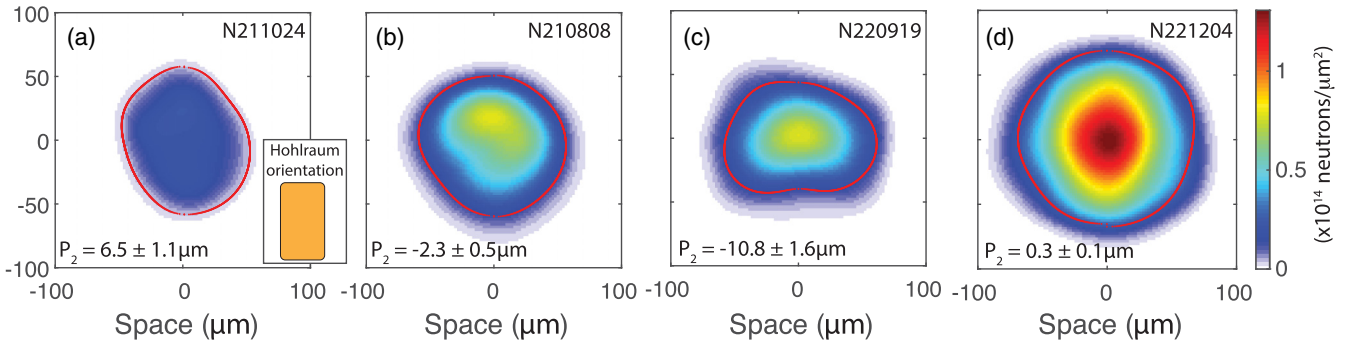

FIG. 3. Equatorial view of the time-integrated neutron emission showing the impact of low-mode asymmetries on the fusion yield for pairs of experiments conducted with (a) and (b) 1.9 MJ of laser energy and (c) and (d) 2.05 MJ of laser energy. The 17% contour of emission is denoted by the red solid line. The inset in (a) shows the hohlraum orientation with respect to the image, and for each experiment the mode 2 amplitude P_2 is given. The mode 1 amplitude for each experiment is given in Fig. 2.

Fig. 2, and the mode 2 asymmetry. Simulations indicate that the 17% contour of neutron emission is a useful quantity to compare the relative morphology of the neutron-emission volume that produces greater than 88% of the total emission [29]. In models that capture the dynamics of the burn, the choice of 17% contour to estimate the emission volume leads to inferences of hot spot pressures and masses that are within 10%–20% of the peak values.

Experiment N211024 was an attempt to repeat the 1.9-MJ experiment N210808 and resulted in a total fusion yield of 0.43 ± 0.02 MJ as compared to 1.3 ± 0.07 MJ for N210808. Experiment N211024 was observed to have a P_2 amplitude of 6.5 ± 1.1 μm as compared to N210808 with a P_2 amplitude of -2.3 ± 0.5 μm. Scalings obtained from simulations indicate that the approximately 3× increase in the $|P_2|$ amplitude is expected to reduce the fusion performance of N211024 by approximately 0.6× as compared to N210808. This, in conjunction with the mode 1 asymmetry difference as seen in Fig. 2, is the dominant degradation that contributes to the fusion yield of N211024 being approximately 30% of N210808 [46].

In contrast, as seen in Fig. 3(c), N220919 was the first experiment conducted with 2.05 MJ of laser energy and had a $|P_2|$ magnitude of 10.8 ± 1.6 μm. This is a larger mode 2 asymmetry than observed on N211024, but the implosion still produced 1.2 ± 0.06 MJ of fusion yield. Using the prior P_2 sensitivity of the 1.9-MJ laser design, this level of P_2 asymmetry is expected to reduce the 1.3 MJ of fusion yield obtained on N210808 by more than 10×. The modest, approximately 10% reduction in yield on N220919 relative to N210808, despite the nearly 2× increase in the P_2 asymmetry from N211024, is direct evidence that the design changes associated with 2.05 MJ have increased the ITFX and yield amplification allowing for higher yields to be obtained despite the presence of degradations that would have significantly degraded the prior 1.9-MJ design. To improve the symmetry following the N220919 experiment, an increase in the wavelength separation of the inner and outer laser cones from 2.5 Å to 2.75 Å was made [15]. This increases the relative amplitude of the equatorial x-ray drive by transferring more energy from the outer to inner laser cones.

As seen in Fig. 3(d), this change resulted in a near round hot spot with a reduced P_2 asymmetry of 0.3 ± 0.1 μm and a fusion yield of 3.1 ± 0.16 MJ. The improvement in mode 2 hot spot symmetry between N220919 and N221204 is found to be the primary reason for the 2.6× increase in fusion yield as these experiments had comparable levels of mode 1 asymmetry and hot spot mix. In contrast, this level of P_2 asymmetry is estimated to degrade the 1.9-MJ design by approximately 8×.

C. Areal density

Further insight into the efficacy of the improvements of the 2.05-MJ compared to the 1.9-MJ laser energy design can be gained by the observed increase in the DSR related to the increase in the areal density of the DT hot spot and fuel. As described in the companion paper [6], one of the goals of the 2.05-MJ design was to further increase the total DT areal density ρR_{DT} at stagnation from prior work, in order to increase the ITFX and yield amplification.

As discussed in Sec. III, the neutron-emission-weighted areal density of the DT fuel can be inferred from experimental observations of the DSR. In the experiments discussed here, the dominant contribution to the DSR is from the DT fuel, followed by the DT hot spot with a small contribution from the remaining ablator; for inertial confinement of the igniting hot spot the total areal density is important. To account for angular variations in the areal density when comparing experiments, multiple measurements of the DSR for each experiment are averaged over the solid angle of emission and a so-called 4π average DSR value is used.

As previously discussed, experiments which approach the ignition threshold experience sustained α-particle self-heating which causes the vast majority of neutrons to be produced as the hot spot expands [47]. Higher levels of self-heating allow for the neutron emission to be sustained to larger hot spot radii, thereby causing the neutron-emission-weighted areal densities to decrease. This dynamic explains the trend displayed by the circles in Fig. 4 that indicates for the 1.9-MJ design, as the fusion yield increases the emission-weighted neutron radius and DSR are observed to increase and decrease, respectively. Therefore, to compare the relative increase in the ρR_{DT} between the 1.9-MJ and 2.05-MJ laser energy designs it is important to compare experiments at comparable yield and hot spot radii.

As seen in Fig. 4, the first 2.05-MJ laser energy experiment, N220919, achieved a similar yield and emission-weighted

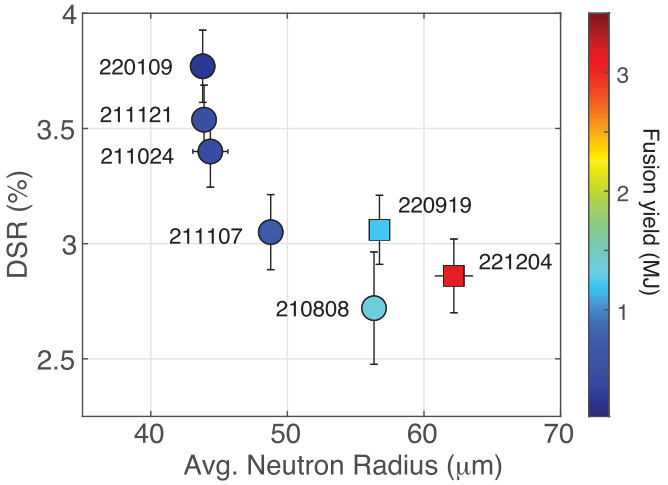

FIG. 4. The 4π averaged downscattered ratio vs the average radius of neutron emission for the 1.9-MJ design (circles) and 2.05-MJ design (squares). The color of the datum corresponds to the fusion yield of the experiment.

hot spot radius as N210808 (the highest-performing 1.9-MJ design) but with a 4π averaged DSR of $3.06 \pm 0.14\%$ as compared to $2.72 \pm 0.24\%$. Additionally, Fig. 4 shows that for the highest-fusion-yield experiment, N221204, a larger neutron-emission radius was achieved than for N210808, while at the same time achieving a higher DSR. Both of these observations are consistent with the design goal of the 2.05-MJ design to achieve a higher-yield amplification by reaching a higher areal density at stagnation. Following Eq. (1), if the level of observed areal density increase at a fusion yield of approximately 1.2 MJ is consistent with that achieved at minimum volume or no-α conditions, then the average increase in the $\mathrm{ITFX}_{\mathrm{no}\,\alpha}$ and Y_{amp} between the 1.9-MJ and 2.05-MJ laser designs is estimated to be $1.28\times$ and $3.4\times$, respectively. These estimates only consider how the change in areal density impacts the ignition threshold metric and does not yet account for other effects such as low-mode asymmetries and mix which can reduce the $Y_{\mathrm{no}\,\alpha}$.

Future experiments will be conducted to quantify changes in the dynamics from the design changes between the 1.9- and 2.05-MJ laser designs that are not directly observable on integrated ignition experiments. These include measurements of the relative velocities and in-flight symmetry which will help to constrain the expected changes in the ignition threshold metric. Additional experiments using "dudded" fusion fuel to minimize the effect of α-particle self-heating will also inform the improvement of $\rho R_{\mathrm{DT\,no}\,\alpha}$ [48].

D. Ion temperature, burn width, and hot spot mass

Figure 5 shows the evolution in the plasma temperature, the neutron-emission duration, and the DT plasma mass change with increasing fusion yield for three experiments that span the range of yields achieved in the 1.9-MJ and 2.05-MJ laser energy designs. Figure 5(a) shows that as the yield increases from 0.25 MJ on N220109 to 3.1 MJ on N221204 the neutron spectra broaden significantly. The apparent DT ion temperature associated with the neutron spectra width more than doubles, increasing from 6.04 ± 0.15 to 13.1 ± 0.74 keV. This dramatic increase in temperature is consistent with α-particle self-heating initially dominating the radiative and expansion losses. Figure 5(b) shows that, as previously predicted and observed, the full width at half maximum (FWHM) of the neutron-emission duration decreases from 104 to 74 ps as the yield increases from 0.25 to 3.1 MJ. This observation is consistent with observations and simulations which show that the FWHM neutron-emission duration decreases owing to the rapid increase in hot spot pressure upon ignition as the temperature rapidly increases due to α-particle hot spot self-heating [49]. Furthermore, as the temperature increases, more and more mass is ablated from the cooler surrounding dense shell of DT fuel into the higher-temperature "hot spot" where fusion occurs. Increasing the contributing DT mass, while increasing the temperature, in turn boosts the α heating and pressure of the hot spot. This continues until the resulting higher values of PdV/dt expansion losses eventually blow the "hot spot" apart. This rapid increase in temperature and pressure leads to a shortening of the FWHM duration of fusion energy production with increasing yields. The mass of the reacting hot spot can be estimated using an emission-weighted static model [17,50] In this model, an average DT density is inferred using the observed yield T_{ion}, burn duration, and emis-

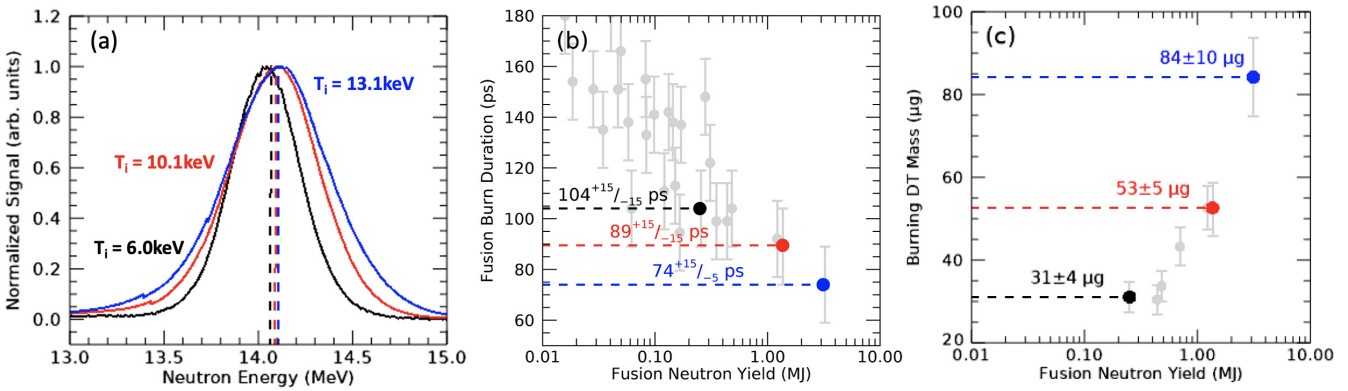

FIG. 5. (a) Neutron spectra and apparent DT ion temperature, from 1.9-MJ laser energy experiments N220109 (black) and N210808 (red) and from a 2.05-MJ laser energy experiment N221204 (blue). (b) Neutron-emission duration as fusion yield. (c) Inferred hot spot mass for 1.9- and 2.05-MJ laser experiments. In (b) and (c) experiments N220109 (black), N210808 (red), and N221204 (red) are highlighted.

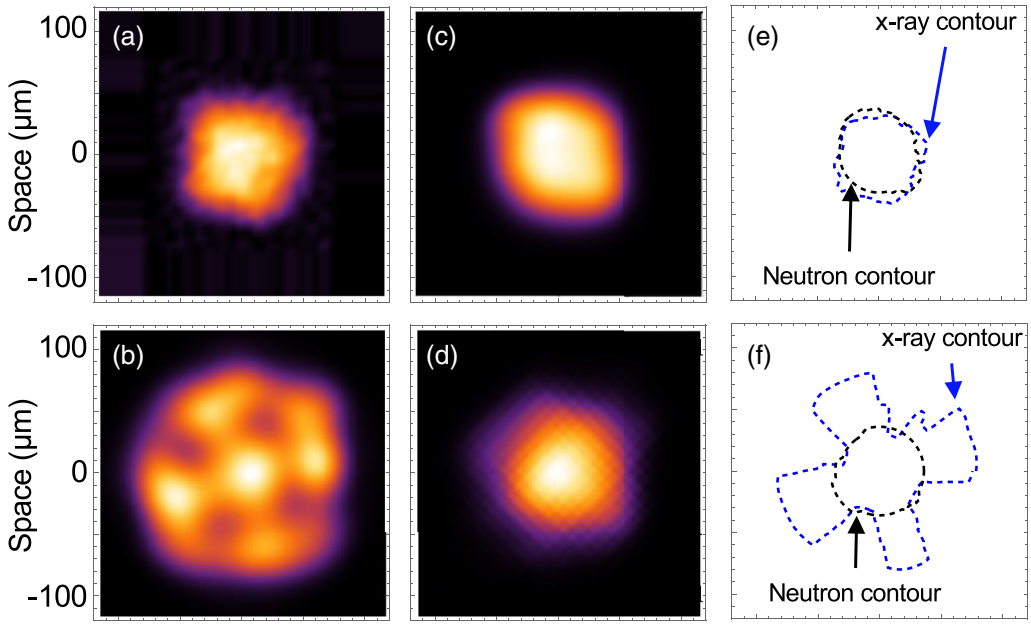

FIG. 6. X-ray- and neutron-emission measurements from (a), (c), and (e) N210808 and (b), (d), and (f) N221204, with time-integrated x-ray emission (greater than 10 keV) from (a) N210808 and (b) N221204 and time-integrated neutron emission from (c) N210808 and (d) N221204. Also shown is a comparison of contours that enclosed 50% of the x-ray and neutron emission for (e) N210808 and (f) N221204. Further details of the x-ray imaging diagnostic are given in the Appendix.

sion volume using the relationship $y = n_{\mathrm{D}} n_{\mathrm{T}} \langle \sigma v \rangle V \tau$. Here y is the neutron yield, V is the volume of the 17% contour of neutron emission, and τ is the FWHM of neutron emission. Bosch-Hale reactivity, which is a strong function of T_{ion}, is used to estimate $\langle \sigma v \rangle$ and n_{D} and n_{T} are equivalent for a 50:50 DT fuel mixture. Once the ion density is inferred, it can be used with the measurement of the plasma volume to estimate the reacting DT plasma mass. This methodology gives reasonable agreement with the mass of the reacting plasma at peak neutron production observed in dynamic calculations [47]. Figure 5(c) indicates that as the yield and temperature increase from N220109 to N221204, the hot spot mass is inferred to increase nearly 3× to 84 ± 10 μg or approximately 40% of the initial DT ice mass. For N221204, over the emission duration, the fraction of the total DT fuel which fuses and burns is approximately 4.3%. Analytic estimates [4] and more detailed estimates from radiation hydrodynamic calculations [29,51] indicate that for inertial confinement fusion, the maximum fraction of fuel that can be burned is related to the hot spot DT density, temperature, and confinement time. The relative scaling of the burn fraction ϕ with increasing areal density and temperature is discussed in more detail in the companion paper [1]. In the robustly burning regime where T reaches near the maximum in the DT reactivity (20 to 40 keV), the burnup fraction is expected to scale as $\phi = \rho R/(\rho R + 6)$, where the areal density ρR is in units of g/cm^2 [4]. If the temperature could be increased to this level, and for a total ρR before α heating of 1.4 g/cm^2 (estimated value of ρR for N221204), this scaling would estimate a $\phi \approx 20\%$.

E. X-ray and neutron observations

As the fusion yield and target gain increased, a significant change in the relative morphology of the x-ray and neutron emission was observed. Understanding such changes is important as they can inform our understanding of symmetry, coupling, burn dynamics, and important quantities such as x-ray-emission duration.

Figures 6(a)–6(d) show the time-integrated self-emission data obtained using x-ray and neutron imagers for experiments N210808 ($E_{\mathrm{laser}} = 1.9$ MJ) and N221204 ($E_{\mathrm{laser}} =$ 2.05 MJ and the 6-μm-thicker capsule). To allow for a direct comparison, the neutron images have been oriented to match the line of sight of the x-ray image, specifically at $(\theta, \phi) = (7^\circ, 180^\circ)$, with the polar angle θ measured in degrees from the top of the target chamber and the azimuthal angle ϕ expressed in degrees. For N210808, Figs. 6(a) and 6(c) show that the x-ray and neutron emission are similar in size and shape. However, comparing the x-ray emission of N221204 in Fig. 6(b) to the neutron emission in Fig. 6(d) shows that the x-ray emission has evolved into a fourfold pattern with a central spot and expanded to a much larger size than the neutron emission.

To better understand how the morphology evolves as the fusion yield increases from 1.3 to 3.1 MJ, Figs. 6(d) and 6(e) show the overlay of contours that enclose 50% of the total of the neutron- and x-ray-emitting regions for N210808 and N221204, respectively. In the case of N221204, the x-ray contour traces the fourfold pattern far outside the neutron contour. This is evidence that this part of the x-ray-emitting volume originates from the higher-Z ablator material that surrounds the DT fuel and emits strongly in x rays but does not produce fusion burn. The x-ray-emission volume is estimated to be 12% larger than the neutron-emission volume in the case of N210808 and 5× larger than the neutron-emission volume in the case of N221204. This stark difference in morphology suggests that for the 2.05-MJ laser energy design, the conditions

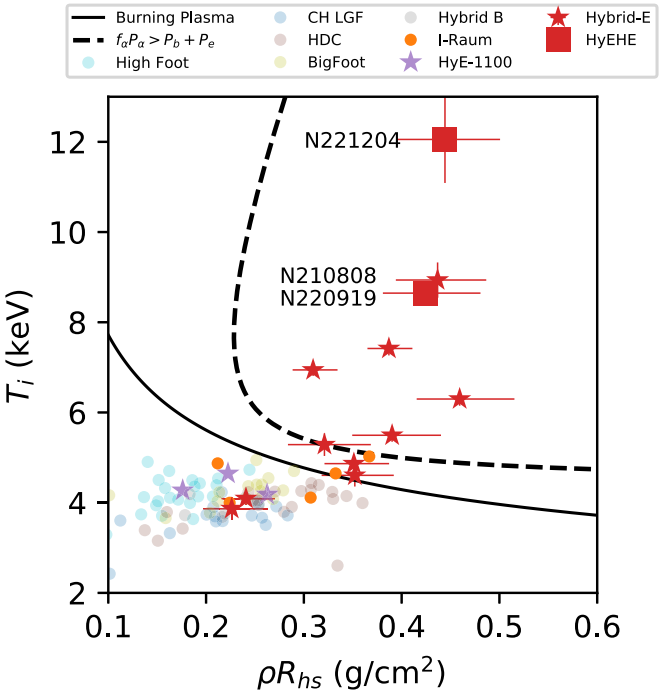

FIG. 7. Hot spot ion temperature and areal density. Thresholds for the burning-plasma criterion (solid line) and static self-heating (dashed line) are shown with NIF data. Here the ion temperature is inferred from the width of the DD neutron spectra.

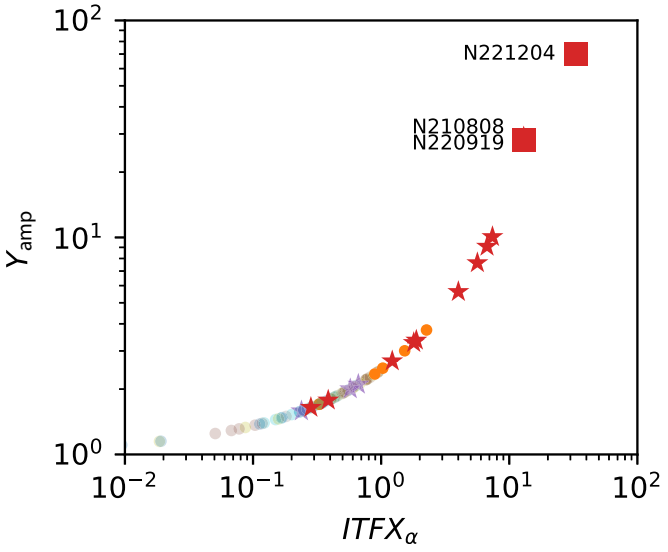

FIG. 8. Inferred yield amplification and ITFX$_\alpha$ for NIF experiments culminating in N221204.

and x-ray emissivity of the surrounding ablator were significantly different than for the 1.9-MJ laser design. This could arise from both differences in the central hot spot pressure and temperature that were achieved as well as from differences in the composition, density, and temperature conditions of the surrounding ablator. Finally, we note that the fourfold pattern in the x-ray image of N221204 suggests that asymmetries still exist, potentially arising from differences in the inner laser cone transmission that lead to azimuthal radiation flux asymmetries. Correcting this in future work could improve energy coupling and decrease areal density variations to further improve performance.

V. INFERRED CONDITIONS AND METRICS

Conditions reached in the hot spot are important for evaluating implosion improvement and burn physics. Here we follow the hot spot condition inference methodology developed in Refs. [17,50,52]. A useful parameter space for evaluating the hot spot conditions is the ion temperature T_i and areal density $\rho R_{\rm hs}$ axes as shown in Fig. 7. Here the ion temperature is inferred from the width of the DD neutron spectra. While the width of both the DT and DD spectra can be used as a relative temperature measurements, the DD spectral width is broadened less by velocity flows within the hot spot than the DT spectra due to the difference in the mass of the reactants. As the DD spectral width is less sensitive to the hot spot velocity flows, it is expected to be closer to the thermal temperature. A criterion for reaching the burning plasma regime, where self-heating surpasses the initial PdV work to form the hot spot, can be cast in this space [12] and is shown in Fig. 7 as the solid curve. The first NIF experiments to enter the burning-plasma regime [17] appear with $T_i \sim 5$ keV and $\rho R_{\rm hs} \sim 0.35$ g/cm^2. The variability experiments with several hundred kilojoule yields are the next points which clearly surpass the static self-heating boundary, shown by the dashed curve, which is when α heating exceeds bremsstrahlung and thermal conduction losses but PdV losses on expansion are neglected. The experiments with yields exceeding 1 MJ (N210808 and N220919) that appear at $T_i \sim 9$ keV and $\rho R_{\rm hs} \sim 0.45$ exhibit a modest increase in areal density but a dramatic increase in ion temperature as the hot spot ignites and begins burn propagation [8,19,20]. Experiment N221204 exhibits a further increase in temperature by approximately 3 keV at a similar $\rho R_{\rm hs}$; since the burn occurs during further expansion of the hot spot, the additional hot spot mass and volume are compensating to produce a similar ρR.

Figure 8 shows the experimentally inferred ignition threshold factor with self-heating (ITFX$_\alpha$) [29], its no-α counterpart introduced in Sec. III. Shot N221204 is the farthest to the right and clearly surpasses the ITFX$_\alpha$ achieved previously on N210808. The yield amplification is inferred from Ref. [52] for the lower-performing experiments (less than approximately 10×) and uses simulated values [6] for the experiments with yields above 1 MJ ($Y_{\rm amp} \gtrsim 30$).

Figure 9 shows the hot spot energy and pressure. In experiments where there is self-heating and burn, the quantities with α heating are directly physical and shown in Fig. 9(b). The equivalent quantities that an experiment would have achieved in the absence of self-heating requires an inference [52] and are shown in Fig. 9(a). As in previous figures, N220919 and N221204 are shown by red squares and the contours represent constant values of EP^2 relative to N210808. Experiment N220919 exhibits a similar pressure and energy to N210808 for both burn on and off. For N221204 we observe a substantial increase in the inferred burn-off energy, likely related to the mitigation of low-mode asymmetry that caused significant residual kinetic energy on N220919. In burn-on conditions

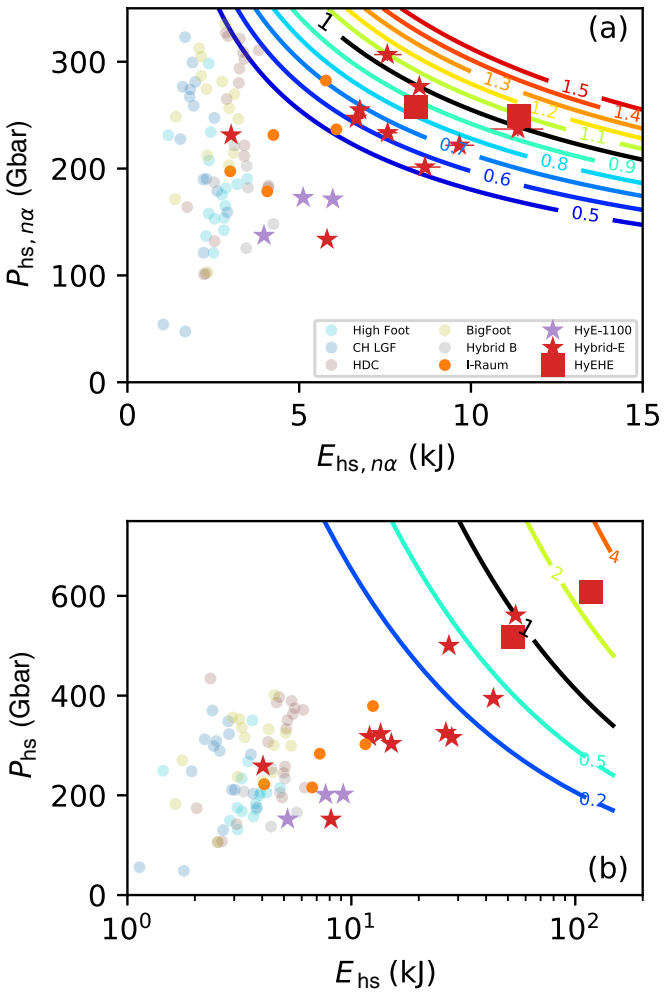

FIG. 9. Inferred hot spot pressure and energy, inferred (a) without the presence of self-heating and (b) directly for the burn-on experiments. Contours of EP^2 relative to N210808 in both cases are shown.

N221204 has a slightly higher inferred pressure than previous NIF shots and, like the hot spot areal density, this is in part due to the fact that the expansion (larger P_0 observed) is reducing the apparent burn-averaged pressure. However, the hot spot energy content is more than twice as large as the previous record experiment N210808.

These inferred quantities provide additional context for the performance of the N221204 experiment increasing substantially from its predecessors. The ITFX_α increase is consistent with the yield amplification from self-heating increasing by more than a factor of 2. The hot spot areal density is approximately maintained while the ion temperature increases approximately 3 keV, which results in an approximately 2× increase in the DT fusion reactivity. Finally, the hot spot pressure increases modestly while the internal energy content of the hot spot increases more than a factor of 2.

VI. CONCLUSION

In summary, the experimental configuration, key observations, inferred conditions, and metrics from the first laboratory experiment to produce more fusion energy than laser energy used to initiate it have been presented. The target gain of this experiment, N221204, is inferred to be 1.5 ± 0.1 with a fraction of burned DT fuel of 4.3% These results were enabled by a design [6] that utilized the approximately 1.08× increase in the available laser energy and a capsule target with an approximately 1.07× thicker ablator to further increase fusion yield by increasing the DT fuel areal density. To achieve this result, activation and neutron imaging diagnostics show that asymmetries in compression arising from laser delivery, hohlraum absorption dynamics, and capsule target wall nonuniformity had to be adjusted and minimized. Observations of an approximately 1.1× increase in the areal density and higher fusion yields from prior work [8], even in the presence of degradations, are consistent with the design goals and previously discussed ignition threshold framework [29]. Consistent with increasing rates of α-particle self-heating, average measurements of the DT neutron spectra show an increase in the inferred ion temperature from 10.1 to 13.1 keV as the fusion yield increased from 1.3 MJ on N210808 to 3.1 MJ on N221204. As the temperature was observed to rise, the radius and mass of the reacting DT hot spot plasma were inferred to increase by approximately 1.1× and approximately 1.6×, respectively. Also consistent with expectations of higher fusion yields and hot spot pressures is the observation of reduced neutron-emission duration from 89^{+15}_{-15} ps to 74^{+15}_{-5} ps. Inferences of the hot spot areal density ρR_{hs} show that as the fusion yield is increased, the DT plasma maintains a nearly constant $\rho R_{\mathrm{hs}} \sim 0.45$ g/cm^2 while the plasma temperature rises rapidly. For N221204, the hot spot is inferred to be approximately twice as far from the static self-heating threshold as N210808. Using nuclear observations, the hot spot energy and pressure were inferred to be approximately 125 kJ and approximately 600 Gbar, respectively, for N221204.

Following N221204, a series of three near repeat experiments were performed. Each repeat obtained a fusion yield greater than 1 MJ while experiencing various levels of low-mode and mix degradations. Future work will study how the sensitivity of this design to known degradations changes from the prior 1.9-MJ laser energy design. Additionally, to achieve still higher fusion yields, future work will focus on utilizing further increases in the available laser energy, developing higher-efficiency radiation cavities [53,54] to increase coupling and higher-compression designs [55]. Additionally, work will be undertaken to better understand how the dynamics and observations, such as the x-ray-emission morphology and duration, change as higher temperatures, pressures, and burn fractions are obtained.

ACKNOWLEDGMENTS

This work was performed under the auspices of U.S. Department of Energy by Lawrence Livermore National Laboratory under Contract No. DE-AC52-07NA27344. This document was prepared as an account of work sponsored by an agency of the U.S. government. Neither the U.S. government nor Lawrence Livermore National Security, LLC, nor any of their employees makes any warranty, expressed or implied, or assumes any legal liability or responsibility for the accuracy, completeness, or usefulness of any information,

TABLE I. Capsule properties for experiments N210808 and N211024 used with 1.9 MJ of laser energy and N220919 and N221204 used with 2.05 MJ of laser energy.

Parameter	N210808	N211024	N220919	N221204
capsule batch number	789-08	789-06	952-03	952-01
capsule mass (μg)	3927	3916	4258	4253.1
inner undoped layer thickness (μm)	6	6.3	7.9	7.7
doped layer thickness (μm)	18.7	18.1	15	15.1
outer undoped layer thickness (μm)	54.9	55	62.5	62.6
capsule dopant areal density (at. % W μm)	7.9	7.6	9.2	9.2
capsule mode 1 (μm)	0.2	0.1	0.07	0.13
capsule surface pits (0–1 μm^3)	270	101	40	69
capsule surface pits (1–3 μm^3)	0	0	1	1
capsule surface pits (>3 μm^3)	0	1	0	0
voids (0-10 μm^3)	0	0	80	20
voids (>10 μm^3)	1	0	12	15
inclusions (<200 μm^3)	31	42	3744	4313
inclusions (>200 μm^3)	5	2	75	105
fill tube diameter (μm)	2	2	2	2
fill tube glue mass (ng)	2.5	0.9	4.1	3.4
fill tube mass deficit (ng)	5.3	5.7	5.1	4.3

apparatus, product, or process disclosed, or represents that its use would not infringe privately owned rights. Reference herein to any specific commercial product, process, or service by trade name, trademark, manufacturer, or otherwise does not necessarily constitute or imply its endorsement, recommendation, or favoring by the U.S. government or Lawrence Livermore National Security, LLC. The views and opinions of authors expressed herein do not necessarily state or reflect those of the U.S. government or Lawrence Livermore National Security, LLC, and shall not be used for advertising or product endorsement purposes.

APPENDIX

Table I summarizes several of the relevant properties for the capsule targets used on the experiments discussed in this work. In these experiments, the capsule was held in place at the center of the hohlraum by two 45-nm Formvar membranes, referred to as a tent [56]. Each capsule had an inner undoped layer of HDC starting at a radius of 1050 μm, followed by a tungsten-doped layer of HDC and an outer undoped layer [57]. On average, the capsules used for the 1.9-MJ laser experiments had a total ablator thickness of 79.5 μm while those used with 2.05 MJ of laser energy had an average thickness of 85.4 μm. The central doped layer attenuates the higher-energy M-band hohlraum x-ray (greater than 1.8–2 keV) emission that passes through the outer undoped HDC. This is to avoid preheating of the inner undoped HDC layer that can increase the Atwood number at the interface, making it more unstable and enhancing the mixing of ablator material into the ice [58]. As noted in Table I, the optical depth of the capsules used with 2.05 MJ of laser energy was increased by 1.19× as compared to those used previously with 1.9 MJ of laser energy. This increase in optical depth is expected to improve the stability of the DT ice and inner undoped HDC interface [6]. However, as noted, this also has the consequence of reducing the ablation front scale length, making the implosion more susceptible to ablation front instabilities. This balance, in conjunction with the differences in instability seeds and changes in growth rates associated with differences in the implosion dynamics (i.e., deceleration rates, etc.), will determine the relative implosion stability. Future experiments will explore the sensitivity of implosion performance to such changes in optical depth of the doped layer.

Table I also details capsule characteristics that can lead to performance degradations. As previously discussed, nonuniformity in the capsule ablator wall thickness can lead to an asymmetry in compression and a reduction in the rate of PdV/dt work and fusion yield [33–35]. Along the principal axis, the wall thickness nonuniformity is fit by a Legendre decomposition and is quantified by the amplitude of the mode 1 coefficient. For all the experiments discussed here, the capsule mode 1 was below 0.2 μm, or approximately 0.25% of the capsule wall thickness. The impact of the capsule nonuniformity on the fusion performance in these experiments will be discussed in detail elsewhere. Higher-atomic-number ablator material that is injected into the reacting hot spot can increase the radiative loss, reducing the temperature and fusion yield [59]. Table I shows the number and volume distribution of surface pits, internal voids, and details of the capsule fill tube assembly. Each of these has been identified as a perturbation which can inject higher-atomic-number ablator material into the reacting hot spot [45,60,61]. Also seen in Table I is that the number of higher-atomic-number inclusions was approximately 100× larger for the capsules used with 2.05 MJ of laser energy and that achieved target gain greater than unity. The impact of these inclusions on both the hot spot and DT fuel-ablator mix is a work in progress. Future experiments using higher-quality capsules with reduced numbers of inclusions will also be performed to quantify the impact.

In this work, the fusion yield is measured using nuclear activation of zirconium foils [62] and through magnetic recoil spectrometry [30]. The uncertainty associated with the fusion yield measurement comes from both systematic and statistical sources. For the yield range of the experiments reported here,

the uncertainty is dominated by a systematic source which arises from the absolute calibration of the detector which measures the nuclear decay signal. This uncertainty is estimated to approximately 5%.

The x-ray image for N221204 was taken using a penumbral imaging setup [63]. The penumbra pinhole diameter and spatial resolution were 220 and 5 μm, respectively, and the pinhole was positioned 140 mm from the target chamber center with an imaging magnification of 44.7×. The data were detected with an image plate and differentially filtered with Ti foils, resulting in a broadband x-ray image with approximately 25 keV emission-weighted average x-ray energy. The x-ray image for N210808 was taken using a pinhole imager with 10-μm-diam pinholes and 12-μm spatial resolution. The data were detected with an image plate and differentially filtered with polycarbonate and Kapton foils, resulting in a broadband x-ray image with approximately 10 keV emission-weighted average x-ray energy.

[1] H. Abu-Shawareb *et al.* (The Indirect Drive ICF Collaboration), Achievement of target gain larger than unity in an inertial fusion experiment, Phys. Rev. Lett. **132**, 065102 (2024).

[2] E. I. Moses, J. Atherton, L. Lagin, D. Larson, C. Keane, B. MacGowan, R. Patterson, M. Spaeth, B. Van Wonterghem, P. Wegner, and R. Kauffman, The National Ignition Facility: Transition to a user facility, J. Phys.: Conf. Ser. **688**, 012073 (2016).

[3] J. Nuckolls, L. Wood, A. Thiessen, and G. Zimmerman, Laser compression of matter to super-high densities: Thermonuclear (CTR) applications, Nature (London) **239**, 139 (1972).

[4] J. Lindl, Development of the indirect-drive approach to inertial confinement fusion and the target physics basis for ignition and gain, Phys. Plasmas **2**, 3933 (1995).

[5] J. D. Lawson, Some criteria for a power producing thermonuclear reactor, Proc. Phys. Soc. B **70**, 6 (1957).

[6] A. L. Kritcher, A. Zylstra, C. Weber, O. Hurricane, D. A. Callahan, D. S. Clark, L. Divol, D. E. Hinkel, K. Humbird, O. Jones *et al.*, following paper, Design of the first fusion experiment to achieve target energy gain $G > 1$, Phys. Rev. E **109**, 025204 (2024).

[7] O. A. Hurricane, D. A. Callahan, D. T. Casey, A. R. Christopherson, A. L. Kritcher, O. L. Landen, S. A. Maclaren, R. Nora, P. K. Patel, J. Ralph, D. Schlossberg, P. T. Springer, C. V. Young, and A. B. Zylstra, Energy principles of scientific breakeven in an inertial fusion experiment, Phys. Rev. Lett. **132**, 065103 (2024).

[8] H. Abu-Shawareb *et al.* (Indirect Drive ICF Collaboration), Lawson criterion for ignition exceeded in an inertial fusion experiment, Phys. Rev. Lett. **129**, 075001 (2022).

[9] A. B. Zylstra, A. L. Kritcher, O. A. Hurricane, D. A. Callahan, K. Baker, T. Braun, D. T. Casey, D. Clark, K. Clark, T. Doppner *et al.*, Record energetics for an inertial fusion implosion at NIF, Phys. Rev. Lett. **126**, 025001 (2021).

[10] A. L. Kritcher, A. B. Zylstra, D. A. Callahan, O. A. Hurricane, C. Weber, J. Ralph, D. T. Casey, A. Pak, K. Baker, B. Bachmann *et al.*, Achieving record hot spot energies with large HDC implosions on NIF in HYBRID-E, Phys. Plasmas **28**, 072706 (2021).

[11] O. A. Hurricane, D. A. Callahan, P. T. Springer, M. J. Edwards, P. Patel, K. Baker, D. T. Casey, L. Divol, T. Döppner, D. E. Hinkel *et al.*, Beyond alpha-heating: Driving inertially confined fusion implosions toward a burning-plasma state on the National Ignition Facility, Plasma Phys. Control. Fusion **61**, 014033 (2019).

[12] O. A. Hurricane, P. T. Springer, P. K. Patel, D. A. Callahan, K. Baker, D. T. Casey, L. Divol, T. Döppner, D. E. Hinkel, M. Hohenberger *et al.*, Approaching a burning plasma on the NIF, Phys. Plasmas **26**, 052704 (2019).

[13] S. Le Pape, L. F. Berzak Hopkins, L. Divol, A. Pak, E. L. Dewald, S. Bhandarkar, L. R. Bennedetti, T. Bunn, J. Biener, J. Crippen *et al.*, Fusion energy output greater than the kinetic energy of an imploding shell at the National Ignition Facility, Phys. Rev. Lett. **120**, 245003 (2018).

[14] J. E. Ralph, O. Landen, L. Divol, A. Pak, T. Ma, D. A. Callahan, A. L. Kritcher, T. Döppner, D. E. Hinkel, C. Jarrott *et al.*, The influence of hohlraum dynamics on implosion symmetry in indirect drive inertial confinement fusion experiments, Phys. Plasmas **25**, 082701 (2018).

[15] P. Michel, L. Divol, E. A. Williams, S. Weber, C. A. Thomas, D. A. Callahan, S. W. Haan, J. D. Salmonson, S. Dixit, D. E. Hinkel, M. J. Edwards, B. J. MacGowan, J. D. Lindl, S. H. Glenzer, and L. J. Suter, Tuning the implosion symmetry of ICF targets via controlled crossed-beam energy transfer, Phys. Rev. Lett. **102**, 025004 (2009).

[16] D. J. Strozzi, D. S. Bailey, P. Michel, L. Divol, S. M. Sepke, G. D. Kerbel, C. A. Thomas, J. E. Ralph, J. D. Moody, and M. B. Schneider, Interplay of laser-plasma interactions and inertial fusion hydrodynamics, Phys. Rev. Lett. **118**, 025002 (2017).

[17] A. B. Zylstra, O. A. Hurricane, D. A. Callahan, A. L. Kritcher, J. E. Ralph, H. F. Robey, J. S. Ross, C. V. Young, K. L. Baker, D. T. Casey *et al.*, Burning plasma achieved in inertial fusion, Nature (London) **601**, 542 (2022).

[18] A. L. Kritcher, C. Young, H. F. Robey, C. R. Weber, A. B. Zylstra, O. A. Hurricane, D. A. Callahan, J. E. Ralph, J. S. Ross, K. L. Baker *et al.*, Design of implosions reaching the burning plasma regime, Nat. Phys. **18**, 251 (2022).

[19] A. L. Kritcher, A. B. Zylstra, D. A. Callahan, O. A. Hurricane, C. R. Weber, D. S. Clark, C. V. Young, J. E. Ralph, D. T. Casey, A. Pak *et al.*, Design of an inertial fusion experiment exceeding the Lawson criterion for ignition, Phys. Rev. E **106**, 025201 (2022).

[20] A. B. Zylstra, A. L. Kritcher, O. A. Hurricane, D. A. Callahan, J. E. Ralph, D. T. Casey, A. Pak, O. L. Landen, B. Bachmann, K. L. Baker *et al.*, Experimental achievement and signatures of ignition at the National Ignition Facility, Phys. Rev. E **106**, 025202 (2022).

[21] J. M. Di Nicola, T. Bond, M. Bowers, L. Chang, M. Hermann, R. House, T. Lewis, K. Manes, G. Mennerat, B. MacGowan *et al.*, The National Ignition Facility: Laser performance status and performance quad results at elevated energy, Nucl. Fusion **59**, 032004 (2018).

[22] J.-M. G. Di Nicola, S. T. Yang, T. C. Bond, M. W. Bowers, L. S. Chang, S. J. Cohen, M. A. Erickson, C. V. Filip, J. A. Folta, A. D. Handler *et al.*, in *High Power Lasers for Fusion Research VI*, edited by A. A. S. Awwal and C. L. Haefner, SPIE Proc. Vol. 11666 (SPIE, Bellingham, 2021), p. 1166604.

[23] J. L. Kline, K. Widmann, A. Warrick, R. E. Olson, C. A. Thomas, A. S. Moore, L. J. Suter, O. Landen, D. Callahan, S. Azevedo *et al.*, The first measurements of soft x-ray flux from ignition scale Hohlraums at the National Ignition Facility using DANTE (invited), Rev. Sci. Instrum. **81**, 10E321 (2010).

[24] M. S. Rubery, G. E. Kemp, M. C. Jones, N. Pelepchan, W. C. Stolte, and J. Heinmiller, Soft x-ray power diagnostics for fusion experiments at NIF, Omega, and Z facilities, Rev. Sci. Instrum. **94**, 031101 (2023).

[25] E. L. Dewald, K. M. Campbell, R. E. Turner, J. P. Holder, O. L. Landen, S. H. Glenzer, R. L. Kauffman, L. J. Suter, M. Landon, M. Rhodes *et al.*, Dante soft x-ray power diagnostic for National Ignition Facility, Rev. Sci. Instrum. **75**, 3759 (2004).

[26] M. S. Rubery, M. D. Rosen, N. Aybar, O. L. Landen, L. Divol, C. V. Young, C. Weber, J. Hammer, J. D. Moody, A. S. Moore, A. L. Kritcher, A. B. Zylstra, O. Hurricane, A. E. Pak, S. MacLaren, G. Zimmerman, J. Harte, and T. Woods, Hohlraum reheating from burning NIF implosions, Phys. Rev. Lett. **132**, 065104 (2024).

[27] O. A. Hurricane, D. T. Casey, O. Landen, A. L. Kritcher, R. Nora, P. K. Patel, J. A. Gaffney, K. D. Humbird, J. E. Field, M. K. G. Kruse *et al.*, An analytic asymmetric-piston model for the impact of mode-1 shell asymmetry on ICF implosions, Phys. Plasmas **27**, 062704 (2020).

[28] R. Betti, K. Anderson, V. N. Goncharov, R. L. McCrory, D. D. Meyerhofer, S. Skupsky, and R. P. J. Town, Deceleration phase of inertial confinement fusion implosions, Phys. Plasmas **9**, 2277 (2002).

[29] J. D. Lindl, S. W. Haan, O. L. Landen, A. R. Christopherson, and R. Betti, Progress toward a self-consistent set of 1D ignition capsule metrics in ICF, Phys. Plasmas **25**, 122704 (2018).

[30] D. T. Casey, J. A. Frenje, M. G. Johnson, F. H. Séguin, C. K. Li, R. D. Petrasso, V. Yu. Glebov, J. Katz, J. Magoon, D. D. Meyerhofer *et al.*, The magnetic recoil spectrometer for measurements of the absolute neutron spectrum at OMEGA and the NIF, Rev. Sci. Instrum. **84**, 043506 (2013).

[31] P. T. Springer, O. A. Hurricane, J. H. Hammer, R. Betti, D. A. Callahan, E. M. Campbell, D. T. Casey, C. J. Cerjan, D. Cao, E. Dewald *et al.*, A 3D dynamic model to assess the impacts of low-mode asymmetry, aneurysms and mix-induced radiative loss on capsule performance across inertial confinement fusion platforms, Nucl. Fusion **59**, 032009 (2019).

[32] G. A. Kyrala, J. L. Kline, S. Dixit, S. Glenzer, D. Kalantar, D. Bradley, N. Izumi, N. Meezan, O. Landen, D. Callahan *et al.*, Symmetry tuning for ignition capsules via the symcap technique, Phys. Plasmas **18**, 056307 (2011).

[33] H. G. Rinderknecht, D. T. Casey, R. Hatarik, R. M. Bionta, B. J. MacGowan, P. Patel, O. L. Landen, E. P. Hartouni, and O. A. Hurricane, Azimuthal drive asymmetry in inertial confinement fusion implosions on the National Ignition Facility, Phys. Rev. Lett. **124**, 145002 (2020).

[34] D. T. Casey, B. J. MacGowan, J. D. Sater, A. B. Zylstra, O. L. Landen, J. Milovich, O. A. Hurricane, A. L. Kritcher, M. Hohenberger, K. Baker *et al.*, Evidence of three-dimensional asymmetries seeded by high-density carbon-ablator nonuniformity in experiments at the National Ignition Facility, Phys. Rev. Lett. **126**, 025002 (2021).

[35] B. J. MacGowan, O. L. Landen, D. T. Casey, C. V. Young, D. A. Callahan, E. P. Hartouni, R. Hatarik, M. Hohenberger, T. Ma, D. Mariscal *et al.*, Trending low mode asymmetries in NIF capsule drive using a simple viewfactor metric, High Energy Density Phys. **40**, 100944 (2021).

[36] J. L. Milovich, D. C. Casey, B. MacGowan, D. Clark, D. Mariscal, T. Ma, K. Baker, R. Bionta, K. Hahn, A. Moore *et al.*, Understanding asymmetries using integrated simulations of capsule implosions in low gas-fill hohlraums at the National Ignition Facility, Plasma Phys. Control. Fusion **63**, 025012 (2021).

[37] C. B. Yeamans and D. L. Bleuel, The spatially distributed neutron activation diagnostic FNADs at the National Ignition Facility, Fusion Sci. Technol. **72**, 120 (2017).

[38] R. M. Bionta, G. P. Grim, K. D. Hahn, E. P. Hartouni, E. A. Henry, H. Y. Khater, A. S. Moore, and D. J. Schlossberg, Real-time nuclear activation detectors for measuring neutron angular distributions at the National Ignition Facility (invited), Rev. Sci. Instrum. **92**, 043527 (2021).

[39] D. T. Casey, O. L. Landen, E. Hartouni, R. M. Bionta, K. D. Hahn, P. L. Volegov, D. N. Fittinghoff, V. Geppert-Kleinrath, C. H. Wilde, J. L. Milovich *et al.*, Three dimensional low-mode areal-density non-uniformities in indirect-drive implosions at the National Ignition Facility, Phys. Plasmas **28**, 042708 (2021).

[40] R. Hatarik *et al.*, Analysis of the neutron time-of-flight spectra from inertial confinement fusion experiments, J. Appl. Phys. **118**, 184502 (2015).

[41] A. S. Moore, D. J. Schlossberg, E. P. Hartouni, D. Sayre, M. J. Eckart, R. Hatarik, F. Barbosa, J. Root, C. Waltz, B. Beeman, M. S. Rubery, and G. P. Grim, A fused silica Cherenkov radiator for high precision time-of-flight measurement of DT γ and neutron spectra (invited), Rev. Sci. Instrum. **89**, 10I120 (2018).

[42] D. Casey, B. MacGowan, O. Hurricane, O. Landen, R. Nora, S. Haan, A. Kritcher, A. Zylstra, J. Ralph, E. Dewald *et al.*, Diagnosing the origin and impact of low-mode asymmetries in ignition experiments at the National Ignition Facility, Phys. Rev. E **108**, L053203 (2023).

[43] A. L. Kritcher, R. Town, D. Bradley, D. Clark, B. Spears, O. Jones, S. Haan, P. T. Springer, J. Lindl, R. H. H. Scott *et al.*, Metrics for long wavelength asymmetries in inertial confinement fusion implosions on the National Ignition Facility, Phys. Plasmas **21**, 042708 (2014).

[44] K. L. Baker, C. A. Thomas, D. T. Casey, M. Hohenberger, S. Khan, B. K. Spears, O. L. Landen, R. Nora, D. T. Woods, J. L. Milovich *et al.*, Hotspot parameter scaling with velocity and yield for high-adiabat layered implosions at the National Ignition Facility, Phys. Rev. E **102**, 023210 (2020).

[45] A. Pak, L. Divol, C. R. Weber, L. F. Hopkins, D. S. Clark, E. L. Dewald, D. N. Fittinghoff, V. Geppert-Kleinrath, M. Hohenberger, S. Le Pape *et al.*, Impact of localized radiative loss on inertial confinement fusion implosions, Phys. Rev. Lett. **124**, 145001 (2020).

[46] L. Divol, *Proceedings of the 61st Annual Meeting of the APS Division of Plasma Physics, Fort Lauderdale, 2019, Meeting Abstracts* (APS, Ridge, 2019), Vol. 2019, p. DI3-001.

[47] A. Pak, L. Divol, D. T. Casey, S. F. Khan, A. L. Kritcher, J. E. Ralph, R. Tommasini, C. Trosseille, A. B. Zylstra, K. L. Baker

et al., Dynamics and power balance of near unity target gain inertial confinement fusion implosions, Phys. Rev. Lett. **131**, 065101 (2023).

[48] K. L. Baker, S. MacLaren, O. Jones, B. K. Spears, P. K. Patel, R. Nora, L. Divol, O. L. Landen, G. J. Anderson, J. Gaffney *et al.*, Alpha heating of indirect-drive layered implosions on the National Ignition Facility, Phys. Rev. E **107**, 015202 (2023).

[49] Y. Kim, K. D. Meaney, H. Geppert-Kleinrath, H. W. Herrmann, T. J. Murphy, C. S. Young, N. M. Hoffman, H. J. Jorgenson, T. Morrow, D. C. Wilson *et al.*, Measurements of fusion reaction history in inertially confined burning plasmas, Phys. Plasmas **30**, 072706 (2023).

[50] A. B. Zylstra, R. Nora, P. Patel, and O. Hurricane, Model validation for inferred hot-spot conditions in National Ignition Facility experiments, Phys. Plasmas **28**, 122703 (2021).

[51] A. R. Christopherson, O. A. Hurricane, C. Weber, A. Kritcher, R. Nora, J. Salmonson, R. Tran, J. Milovich, S. Maclaren, D. Hinkel *et al.*, Alpha-heating analysis of burning plasma and ignition experiments on the National Ignition Facility, Phys. Plasmas **30**, 062705 (2023).

[52] P. K. Patel, P. T. Springer, C. R. Weber, L. C. Jarrott, O. A. Hurricane, B. Bachmann, K. L. Baker, L. F. Berzak Hopkins, D. A. Callahan, D. T. Casey *et al.*, Hotspot conditions achieved in inertial confinement fusion experiments on the National Ignition Facility, Phys. Plasmas **27**, 050901 (2020).

[53] P. Amendt, D. Ho, Y. Ping, V. Smalyuk, S. Khan, J. Lindl, D. Strozzi, R. Tommasini, M. Belyaev, C. Cerjan *et al.*, Ultra-high (>30%) coupling efficiency designs for demonstrating central hot-spot ignition on the National Ignition Facility using a Frustraum, Phys. Plasmas **26**, 082707 (2019).

[54] K. L. Baker, P. A. Amendt, J. S. Ross, V. A. Smalyuk, O. L. Landen, D. D. Ho, S. Khan, S. W. Haan, J. D. Lindl, D. Mariscal *et al.*, First large capsule implosions in a frustum-shaped hohlraum, Phys. Plasmas **30**, 092708 (2023).

[55] D. S. Clark, D. T. Casey, C. R. Weber, O. S. Jones, K. L. Baker, E. L. Dewald, L. Divol, A. Do, A. L. Kritcher, O. L. Landen *et al.*, Exploring implosion designs for increased compression on the National Ignition Facility using high density carbon ablators, Phys. Plasmas **29**, 052710 (2022).

[56] S. R. Nagel, S. W. Haan, J. R. Rygg, M. Barrios, L. R. Benedetti, D. K. Bradley, J. E. Field, B. A. Hammel, N. Izumi, O. S. Jones *et al.*, Effect of the mounting membrane on shape in inertial confinement fusion implosions, Phys. Plasmas **22**, 022704 (2015).

[57] T. Braun, S. O. Kucheyev, S. J. Shin, Y. M. Wang, J. Ye, N. E. Teslich, Jr., C. K. Saw, D. B. Bober, E. M. Sedillo, N. G. Rice *et al.*, Tungsten doped diamond shells for record neutron yield inertial confinement fusion experiments at the National Ignition Facility, Nucl. Fusion **63**, 016022 (2023).

[58] D. S. Clark, S. W. Haan, A. W. Cook, M. J. Edwards, B. A. Hammel, J. M. Koning, and M. M. Marinak, Short-wavelength and three-dimensional instability evolution in National Ignition Facility ignition capsule designs, Phys. Plasmas **18**, 082701 (2011).

[59] T. Ma, P. K. Patel, N. Izumi, P. T. Springer, M. H. Key, L. J. Atherton, L. R. Benedetti, D. K. Bradley, D. A. Callahan, P. M. Celliers *et al.*, Onset of hydrodynamic mix in high-velocity, highly compressed inertial confinement fusion implosions, Phys. Rev. Lett. **111**, 085004 (2013).

[60] A. B. Zylstra, D. T. Casey, A. Kritcher, L. Pickworth, B. Bachmann, K. Baker, J. Biener, T. Braun, D. Clark, V. Geppert-Kleinrath *et al.*, Hot-spot mix in large-scale HDC implosions at NIF, Phys. Plasmas **27**, 092709 (2020).

[61] B. Bachmann, J. E. Ralph, A. B. Zylstra, S. A. MacLaren, T. Döppner, D. O. Gericke, G. W. Collins, O. A. Hurricane, T. Ma, J. R. Rygg *et al.*, Localized mix-induced radiative cooling in a capsule implosion at the National Ignition Facility, Phys. Rev. E **101**, 033205 (2020).

[62] D. L. Bleuel, C. B. Yeamans, L. A. Bernstein, R. M. Bionta, J. A. Caggiano, D. T. Casey, G. W. Cooper, O. B. Drury, J. A. Frenje, C. A. Hagmann *et al.*, Neutron activation diagnostics at the National Ignition Facility (invited), Rev. Sci. Instrum. **83**, 10D313 (2012).

[63] B. Bachmann, T. Hilsabeck, J. Field, N. Masters, C. Reed, T. Pardini, J. R. Rygg, N. Alexander, L. R. Benedetti, T. Döppner *et al.*, Resolving hot spot microstructure using x-ray penumbral imaging (invited), Rev. Sci. Instrum. **87**, 11E201 (2016).